Marine and Petroleum Geology 133 (2021) 105286

Contents lists available at ScienceDirect

Marine and Petroleum Geology

journal homepage: www.elsevier.com/locate/marpetgeo

Dolomitization micro-conditions constraint on dolomite stoichiometry: A case study from the Miocene Huangliu Formation, Xisha Islands, South China Sea

Rui Wang [a], Kefu Yu [a,*], Brian Jones [b], Wei Jiang [a], Shendong Xu [a], Tianlai Fan [a], Yu Zhang [a]

[a] Guangxi Laboratory on the Study of Coral Reefs in the South China Sea, Coral Reef Research Center of China, School of Marine Sciences, Guangxi University, Nanning, 530004, China
[b] Department of Earth and Atmospheric Sciences, University of Alberta, Edmonton, Alberta T5R 3C8, Canada

ARTICLE INFO

Keywords:
Dolomitization
Stoichiometry
Micro-conditions
Island dolostones
Miocene
Xisha Islands

ABSTRACT

The micro-conditions that control dolomitization processes were still not well known in natural environments. Cenozoic "island dolostones" are ideal for examining the processes since they are geologically young and have not experienced deep burial conditions. Miocene dolostones from the Xisha Islands, located in the South China Sea, are similar to those found on Grand Cayman Island, located in the Caribbean Sea. These dolostones are composed of low-Ca dolomite (LCD, < 55 mol % $CaCO_3$; hereafter referred to as %Ca) and high-Ca dolomite (HCD, > 55 %Ca). Individual dolomite crystals are commonly formed entirely of LCD or HCD, and/or HCD cores that are encased by LCD and alternating zones of HCD and LCD (1–10 μm thick). The crystal textures indicate that the LCD and HCD are primary growth features (no obvious recrystallization) that formed as the dolomite replaced the limestone precursor. The compositional features (%Ca in LCD and HCD, average %Ca, and proportion of LCD and HCD) and geochemical parameters (O/C isotopes, Sr, Fe and Mn) of dolomite indicate that the Mg was incorporated into dolomite crystals in an orderly manner that was mainly controlled by the interaction of fluid properties and crystal structure. The fact that dolomite stoichiometry varied laterally and vertically throughout the successions shows that micro-scale physicochemical conditions played a critical role in the evolution of individual dolomite crystals. The similarities between the dolostones of the Xisha Islands and Grand Cayman, which are 15,795 km apart, indicate that the factors that control the micro- and large-scale features of these dolostones must have undergone similar processes or experienced similar physicochemical conditions despite their disparate settings.

1. Introduction

The origin of dolomite [$CaMg(CO_3)_2$] has remained an enigma ever since it was first named and discovered over two hundred years ago (e.g., Van Tuyl, 1916; Budd, 1997; Land, 1985, 1998; Warren, 2000; Machel, 2004; Mckenzie and Vasconcelos, 2009; Gregg et al., 2015; Kaczmarek et al., 2017; Petrash et al., 2017). Despite numerous studies, the precise causes of the pervasive dolomitization of thick successions of limestones, commonly referred to as the "dolomite problem" (e.g., Given and Wilkinson, 1987; Budd, 1997; Machel, 2004), still remains one of the most elusive challenges in geology. Morrow (1982a, 1982b) noted that the fundamental requirements in all dolomitization models are (1) a source of Mg, (2) a delivery system that transports the Mg to the dolomitization site, and (3) conditions, at the site of dolomitization, that foster transformation of the limestones to dolostones. Although the first two criteria have been extensively examined and form the basis of virtually every dolomitization model, including, for example, the tidal pumping, reflux, mixing of seawater and freshwater schemes (e.g., Tucker and Wright, 1990; Budd, 1997; Ren and Jones, 2018), relatively little attention has been paid to the micro-scale conditions that exist at the site of dolomitization.

Cenozoic "island dolostones", found on various islands throughout the oceans of the world (Budd, 1997), are considered ideal candidates for examining the factors that control dolomitization because they have not been subjected to deep burial diagenesis and formed in environments that can be reasonably inferred from their present-day settings (e.

* Corresponding author.
E-mail addresses: kefuyu@scsio.ac.cn, yukefu@gmail.com (K. Yu).

https://doi.org/10.1016/j.marpetgeo.2021.105286
Received 14 November 2020; Received in revised form 30 November 2020; Accepted 10 August 2021
Available online 12 August 2021

g., Budd, 1997; Zhao and Jones, 2012; Ren and Jones, 2018). The thick Miocene to Pleistocene carbonate succession (~1200 m) on the Xisha Islands (South China Sea), for example, includes seven dolostone intervals (DI 1 to 7 as defined by Zhai et al., 2015 and Bi et al., 2018) with some intervals being >200 m thick. These dolostone units are typically thicker than those found on other islands in the Pacific Ocean (e.g., Niue, Kita-Daito-Jima) and Caribbean Sea (e.g., Bonaire, Jamaica, Barbados, Curacao) (Wang et al., 2018a, 2019).

This study focuses on the Miocene dolostones in the Huangliu Formation found in Well CK-2 on Chenhang Dao (Xisha Islands), located in the north part of the South China Sea (Fig. 1). Specifically, this study examines the composition, crystal size, and texture of the dolostones in order to gain insights into the micro-scale conditions that led to their growth and transformation of the limestones to dolostones. Comparison of these dolostones with those of the same age on Grand Cayman (Caribbean Sea), which are 15,795 km from the Xisha Islands, allows an assessment of the factors that were controlled by local (e.g. temperature, Mg/Ca, salinity) as opposed to world-wide conditions (pCO_2, eustatic sea-level, Mg/Ca ratio of ocean waters). Information from high-temperature experiments (e.g. Kaczmarek and Sibley, 2007, 2011; Gregg et al., 2015; Kaczmarek and Thornton, 2017; Cohen and Kaczmarek, 2018) are also integrated into the discussion because of the insights that they provide with respect to the growth of dolomite crystals. The striking similarities between the dolostones of Chenhang Dao and the Cayman Islands indicate that the factors that controlled the micro- and large-scale features of these dolostones must have been similar despite their disparate settings.

2. Geologic setting

The Xisha Islands, located in the northwest part of the South China Sea, encompass numerous atolls that are located on an elevated submarine plateau and surrounded by deep ocean waters (Fig. 1A and B). There, drilling has shown that the thick (up to 1257.2 m) carbonate succession rests on top of Jurassic and/or Cretaceous metamorphic/volcanic rocks (Zhu et al., 2017). Available chronological information (e.g., strontium isotopes, biostratigraphy, paleomagnetism) indicates that the Xisha Platform was initiated ~24 to 19 Ma between the late Oligocene (Yi et al., 2018) and early Miocene (Fan et al., 2020). The platform flourished throughout the middle Miocene before waning during the late Miocene and significantly reducing in size during the Pliocene-Quaternary (e.g. Wu et al., 2014; Shao et al., 2017a, b). The carbonate succession on the Xisha Platform is typically divided into five unconformity-bounded formations that are, in ascending order, the Sanya Formation, Meishan Formation, Huangliu Formation, Yinggehai Formation, and Ledong Formation (Fig. 1C) (Zhao, 2010; Wu et al.,

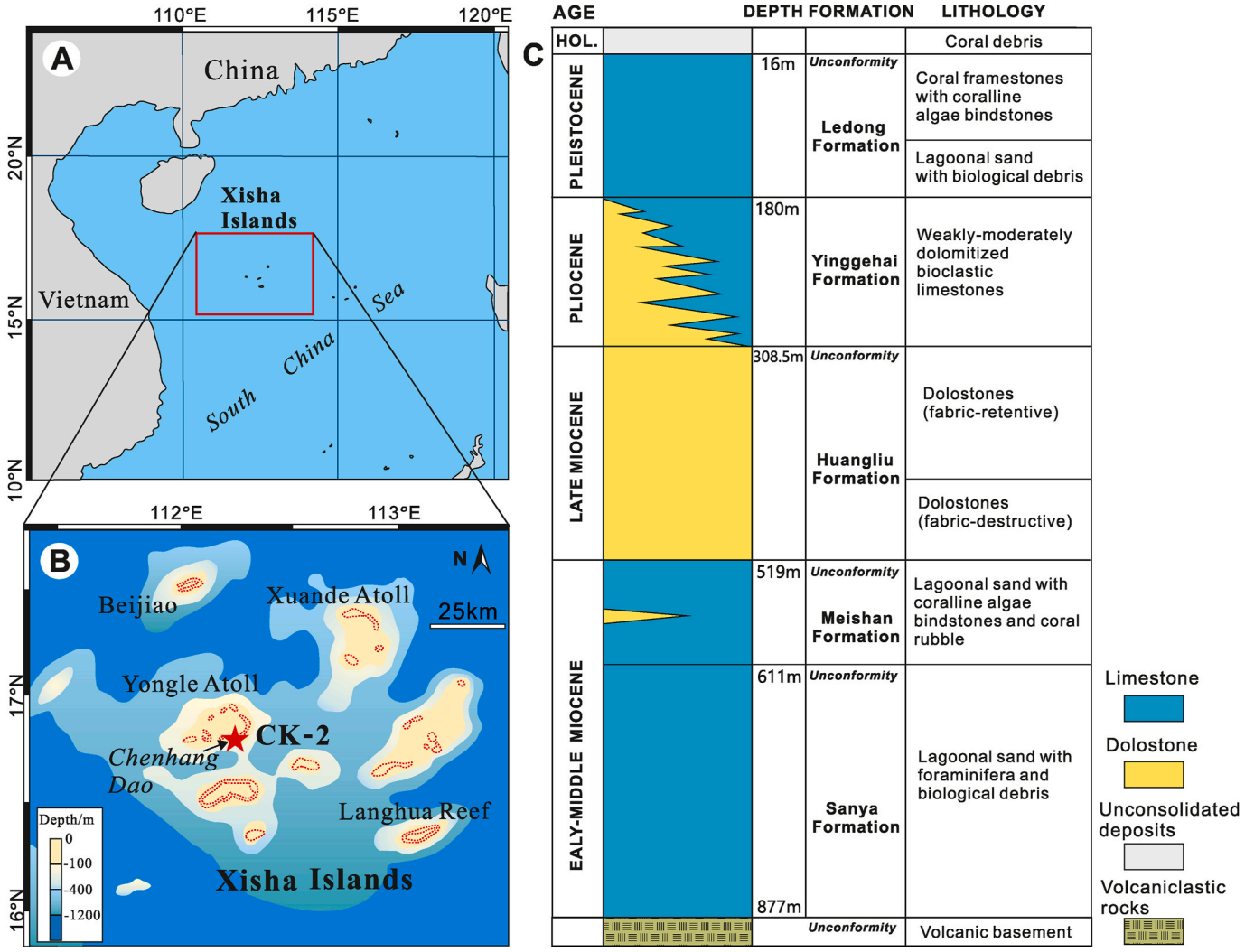

Fig. 1. (A) Location of Xisha Islands (red rectangle) in northwest part of South China Sea. (B) Map showing Xisha Platform surrounded by various deep-water (>1000 m) areas. Red star indicates location of well CK-2. (C) Stratigraphic succession on Xisha Platform based on core from well CK-2. (For interpretation of the references to colour in this figure legend, the reader is referred to the Web version of this article.)

2014; Shao et al., 2017a, b; Wang et al., 2018a). The Miocene Huangliu Formation, with an average thickness of ~235 m, is formed almost entirely of dolostones (Wang et al., 2018a,b).

Well CK-2, on Chenhang Dao (Fig. 1B), drilled in 2013, penetrated the entire carbonate succession (0–873.55 m) before terminating in the volcaniclastic basement (20–35.5 Ma) at a depth of 928.75 m (Zhang et al., 2018, 2020; Jiang et al., 2019; Xu et al., 2019; Fan et al., 2020). The average core recovery from this well was ~70 % with >80 % in most parts. In this well, the Huangliu Formation (210.5 m thick) is located 308.5–519 m below sea level (bsl) (Fig. 1C).

3. Methods

Facies and petrographic analysis of the Huangliu Formation in well CK-2 is based on hand samples and standard thin-sections (126 samples) that were stained with Alizarin Red-S solution. The fabric-retentive dolostones in the Huangliu Formation are described and classified following Dunham (1962).

One hundred and three samples (ca. 1.5 m intervals) were used for X-ray diffraction (XRD). Each sample was thoroughly washed to remove any salt that may still be present. After drying, the samples were ground into a powder (<74 μm) using an agate mortar and pestle. XRD analyses followed the protocol of Jones et al. (2001) with quartz being added to each sample as an internal standard. The samples were analyzed using a Rigaku Ultima IV XRD system with Cu Kα radiation, located at Guangxi University, China, that was operated at 40 kV and 35 mA, scanning from 25° to 38° 2θ with a 0.004° 2θ step size. Dolomite stoichiometry (%Ca) was calculated using the peak-fitting X-ray diffraction (PF-XRD) method of Jones et al. (2001). Following Jones et al. (2001), the dolomite is divided into low-Ca dolomite (LCD: 50–55 %Ca) and high-Ca dolomite (HCD: 55–62 %Ca). The average %Ca is calculated by following formula:

$$Average\ \%Ca = ((\%\ of\ LCD * \%Ca\ in\ LCD) + (\%\ of\ HCD * \%Ca\ in\ HCD))/100$$

Twenty-one polished thin sections were made from samples, at ~10 m intervals, which were devoid of obvious fossil fragments. After coating with carbon, backscatter electron images were obtained using a JEOL 8230 electron microprobe (EMP), located at Guangxi University (China), that was operated with a 10 kV accelerating voltage and 15 nA beam current. Spot analyses were done with 10 s count time on Ca and Mg peaks, and 5 s count time on the backgrounds. A beam diameter of 2 or 5 mm was used to analysis the different zones of the dolomite crystal.

Carbon and oxygen isotopes (103 samples, ca. 1.5 m intervals) were obtained using a Finnigan AT-253 stable isotope mass spectrometer, located at Guangxi University, China. $\delta^{18}O$ and $\delta^{13}C$ values are reported in standard delta (δ) notation in per mil (‰) relative to Vienna Peedee belemnite (VPDB) using the GBW04405 standard ($\delta^{13}C = 0.57$ ‰, $\delta^{18}O = -8.49$ ‰). Multiple measurements (n = 15) of this standard yielded a standard deviation of 0.03 % for $\delta^{13}C$ and 0.08 % for $\delta^{18}O$. The concentrations of Fe, Mn and Sr (103 samples, ca. 1.5 m intervals) were obtained using an inductively coupled plasma emission mass spectrometer (ICP-MS) that is located at Guangxi University, China.

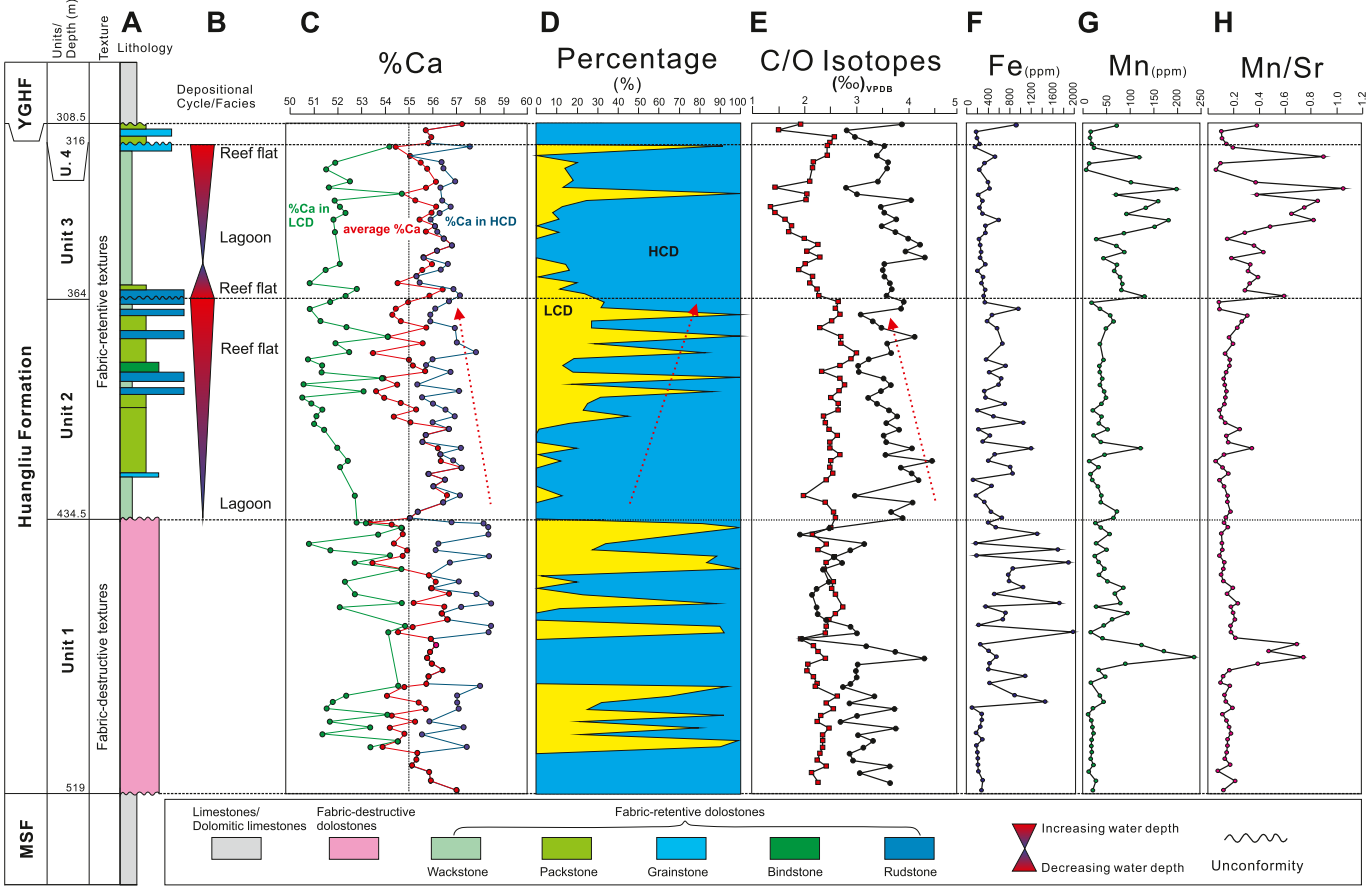

Fig. 2. Composite stratigraphic succession in upper part of well CK-2 in the Xisha Islands (South China Sea). MSF, Meishan Formation; YGHF, Yinggehai Formation. Depth is below sea level (bsl). For the Huangliu Formation, the column shows the stratigraphic variations in (A) Lithology, (B) Depositional cycles and facies, (C) %Ca in the low-Ca dolomite (LCD) and high-Ca dolomite (HCD), and the average %Ca, (D) relative percentage of LCD and HCD, (E) $\delta^{18}O$ and $\delta^{13}O$ (‰) relative to Vienna Peedee belemnite (VPDB), (F) Fe contents, (G) Mn contents and (H) Mn/Sr ratios. Black dashed line represents boundary of each Units. Red dashed line arrow means the general decreasing values of average %Ca and $\delta^{18}O$, and increasing percentage of LCD in Unit 2. (For interpretation of the references to colour in this figure legend, the reader is referred to the Web version of this article.)

4. Results

4.1. Internal stratigraphy of the Huangliu Formation – well CK-2

Wang et al. (2018a) divided the Huangliu Formation into five unconformity-bounded units (1–4) (Fig. 2). Unit 1 (434.5–519 m) is formed of tan, well-indurated medium to coarsely crystalline, fabric-destructive dolostones composed of interlocking anhedral to euhedral dolomite crystals (most 10–60 μm long) and euhedral limpid dolomite crystals (up to 500 μm long, but most 30–140 μm long). Units 2 (364–434.5 m), 3 (316–364 m), and 4 (308.5–316 m), are composed of gray, fine to medium crystalline fabric-retentive dolostones formed of interlocking anhedral to subhedral dolomite (<30 μm long), with limpid dolomite cements (crystals 2–60 μm long) in some pores/cavities. The uppermost beds in units 2, 3 and 4 (~1.5 m, ~1 m and ~50 m thickness respectively) are highlighted by their yellow brown staining.

4.2. Sedimentary facies

The fabric-destructive dolostones of unit 1, with rare fossils apart from scattered coralline algae, is difficult to describe in terms of its original sedimentary facies. In contrast, the fabric-retentive dolostones of units 2, 3, and 4 encompass facies that are indicative of reef flat and lagoonal settings (Fig. 2A and B). The reef flat facies, in the upper part of unit 2 and lower part of unit 3 (362–394 m) and the upper part of unit 3 and all of unit 4 (308.5–318 m) (Fig. 2A), are composed largely of skeletal rudstones (Fig. 4G and H), bindstones (Fig. 4F), and packstones (Fig. 4C) that include corals, rhodoids, red algae (e.g., *Melobesiodideae*), benthic foraminifera, and scattered bivalves, gastropods, and green algae (mainly *Halimeda*). The lagoonal facies, in the lower part of unit 2 (394–434.5 m) and middle section of unit 3 (318–362 m) (Fig. 2A), are formed largely of wackstones (Fig. 4A) and packstones (Fig. 4B, D) that contain red algae fragments (generally < 2 mm), benthic foraminifera (mostly *Amphistegina*), and micritized bio-fragments. Skeletons originally formed of aragonite (e.g., corals, gastropods, bivalves) have generally been partially or completely dissolved, whereas biofragments originally formed of Mg-calcite (e.g., red algae) are well preserved (Fig. 4I).

4.3. Dolomite in Huangliu Formation

4.3.1. Crystal architecture

Backscatter imaging shows that the dolostones from the Huangliu Formation are formed of (1) various mixtures of LCD and HCD, (2) LCD, or (3) HCD (Fig. 5). Many crystals in units 1, 2, and 3 are zoned with "dirty cores" formed of HCD with numerous micropores and calcite inclusions that are encased by LCD (Fig. 5B–D). In contrast, the dolostones in unit 4 are composed solely of HCD crystals (Fig. 5A). In unit 1, the HCD cores in some crystals are encased by a cortex formed of alternating HCD and LCD zones that are each 2–10 μm thick (Fig. 5B). The boundaries between the HCD and LCD zones are sharp. EMP spot analyses shows that the %Ca content of successive HCD and LCD layers typically have a difference of ~4.5–5 %Ca (Fig. 5B–D). Some dolostones in units 1 to 3 are formed entirely of LCD or HCD.

4.3.2. %Ca content

The offset of the d (104) values of dolostones from the Huangliu Formation, which is between 2.88 Å and 2.90 Å, shows that the dolomites are Ca-rich, with a %Ca content of 50.4–58.4 %. For 56 of the samples, two superimposed 104 peaks (Fig. 6A) indicate the presence of two dolomite populations (HCD and LCD) with different %Ca contents (e.g., Lumsden, 1979; Jones et al., 2001), whereas the other 47 samples have single 104 peaks that are indicative of pure HCD or pure LCD. The frequency distribution of %Ca, based on all samples, is also characterized by two modes (Fig. 7A). The two superimposed 104 peaks evident in many of the samples are also matched by double peaks in the basal

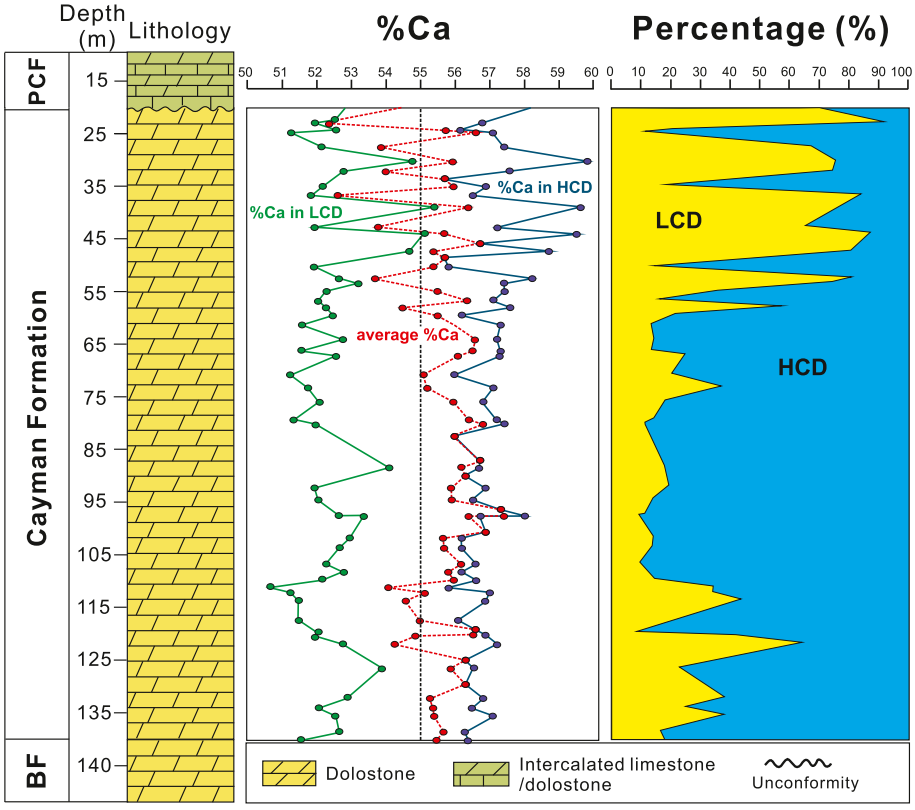

Fig. 3. Dolomite stoichiometry of dolostones in the Cayman Formation from well LV#2, Cayman Island (Caribbean Sea). BF, Brac Formation; PCF, Pedro Castle Formation. Depth is below sea level (bsl).

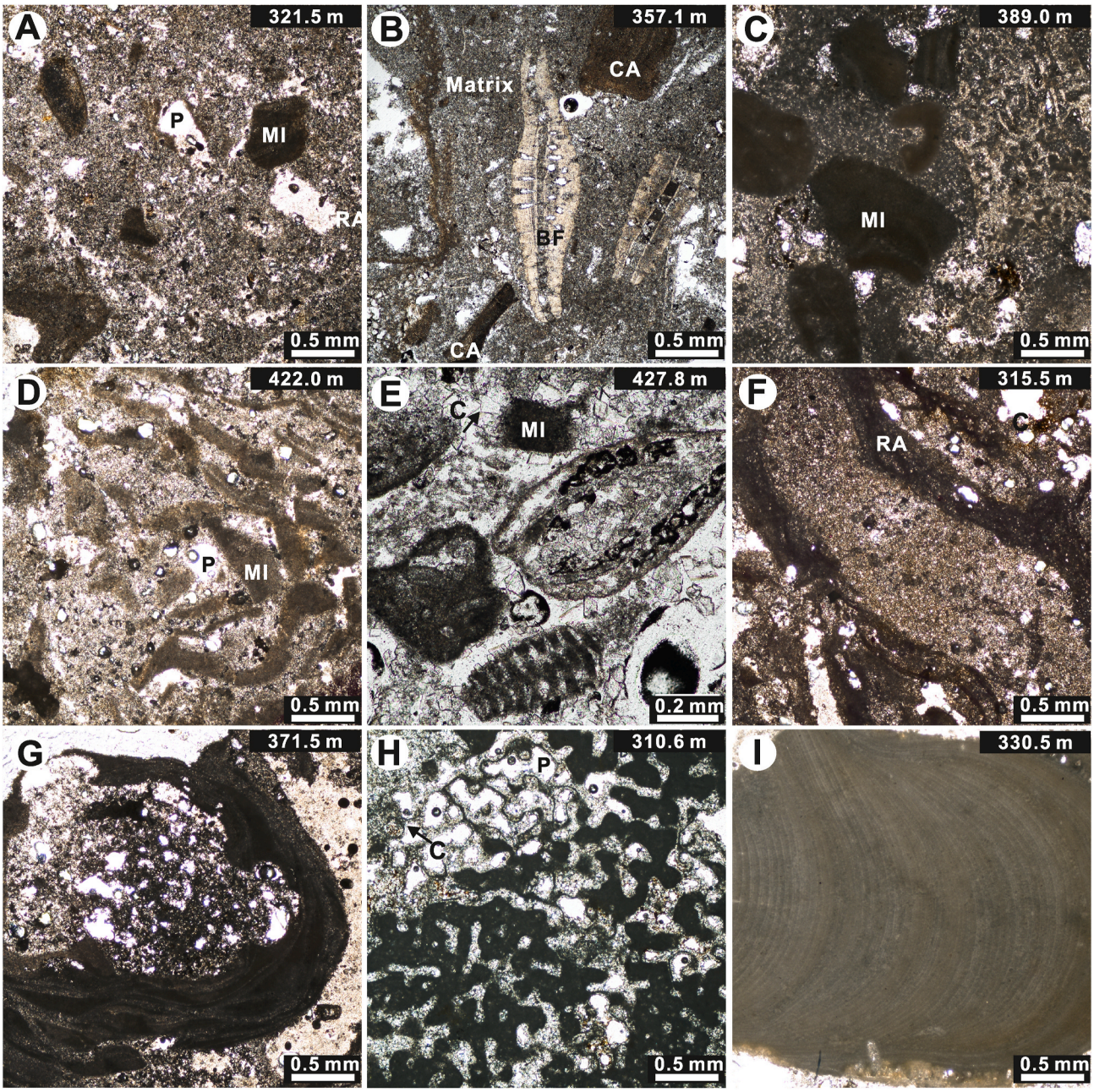

Fig. 4. Thin section photomicrographs (plane polarized light) illustrating petrological features of the fabric-retentive dolostones (units 2 to 4) in the Huangliu Formation of well CK-2 in the Xisha Islands. Depths specified in upper right corner of each image are below present-day sea level. (A) wackstone, note the slight micritization (MI) of scattered broken skeletons. P = pore. (B) wackstone/packstone, matrix-supported or grain-supported, in which coralline algae (CA) and benthic foraminifera (BF) are common. (C) fossilifereouse packstone, most broken skeletons were micritized (MI). (D) packstone, containing many broken shells (?) that were slightly micritized (MI). (E) fossilifereouse grainstone, note the cements (C, black arrow) lining in the intergranular pore. (F) red algae (RA) bindstone, (G) rhodoid (generally > 2 mm) rudstone with matrix between them, (H) coral rudstone, residual coral skeletons were partly micritized with cements lining in the framework pores. (I) coralline algae debris well preserved internal texture. (For interpretation of the references to colour in this figure legend, the reader is referred to the Web version of this article.)

reflection (006) peak and the principal dolomite ordering (015) peak (Fig. 6B).

Overall, there is no obvious correlation between the %Ca in LCD, % Ca in HCD, average %Ca and depth (Fig. 2C). In unit 2, however, there is a progressive vertical increase in the average %Ca (Fig. 2C). The %Ca the LCD ad HCD both fluctuate with depth (Fig. 2C), and the difference between the %Ca content in the LCD and HCD of individual samples is consistently ~4.5 %Ca (Fig. 8A).

4.3.3. Percentages of LCD and HCD

In general, the percentage of LCD (%LCD) tends to be the highest just below the unconformities (Fig. 2D). The %LCD increases with depth in unit 2, whereas in unit 3 the %LCD decreases with depth before once again increasing at a depth of ~350 m (Fig. 2D). Only two of the 103 samples yielded %LCD values between 35 and 75 % and %HCD values between 25 and 65% (Fig. 9A and B). In samples with a high content (75–100 %) of %LCD, the %Ca is typically 52.5–55 %, whereas in samples with a high %HCD content (65–100 %) the %Ca is typically 50–53 % (Fig. 9A and B).

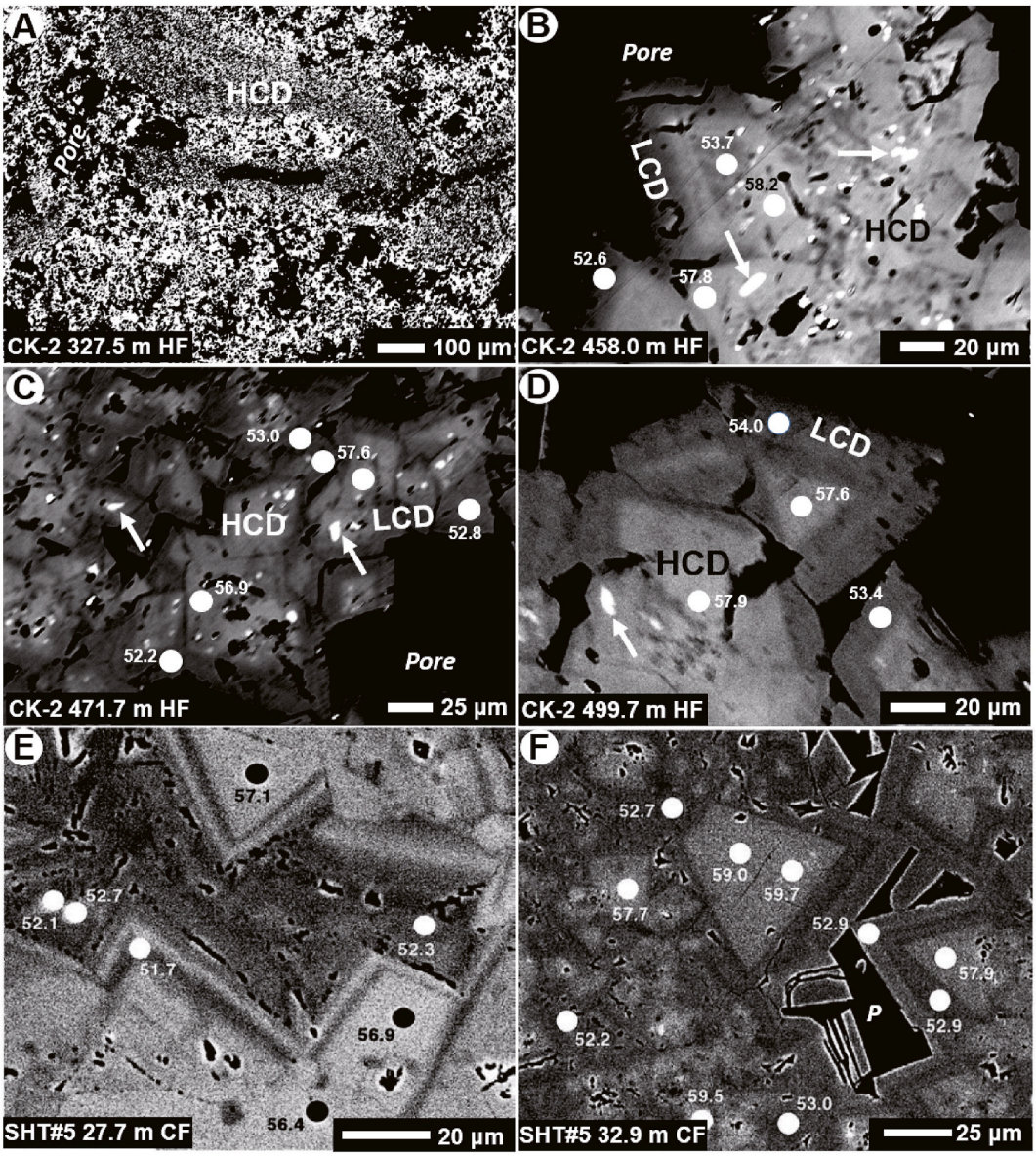

Fig. 5. Backscatter images and EMP spot analysis from the dolostones of the Huangliu Formation (HF), well CK-2, Xisha Islands (A–D) and dolostones of the Cayman Formation (CF), well SHT#5, Grand Cayman (E, F) (E and F images from Jones and Luth, 2002). Light gray = HCD; dark gray = LCD. Depths in lower left corner of each image are below sea level. (A) Almost pure HCD with no obvious LCD. (B) Dolomite crystals formed of alternating LCD (dark gray) and HCD (light gray) zones. (C, D) Euhedral dolomite crystals with HCD cores and LCD cortices. Note calcite inclusions (white arrows) in HCD. (E, F) Dolomite crystals formed of alternating LCD (dark gray) and HCD (light gray) zones. Note that the %Ca content of successive HCD and LCD layers typically have a difference of ~4.5–5 %Ca.

4.4. Geochemistry

Dolostones in the Huangliu Formation (98 samples) yielded $\delta^{18}O$ values from 0.9 to 4.4 ‰ (average 3.3 ‰) and $\delta^{13}C$ values from 1.0 to 3.0 ‰ (average 2.3 ‰) (Fig. 2E). In unit 2, the $\delta^{18}O$ values generally increase with depth (Fig. 2E). The $\delta^{18}O$ values of pure HCD (1.9–4.3 ‰, average 2.9 ‰; n = 39), have a slightly larger range than those of the pure LCD (2.4–4.1 ‰, average 3.1 ‰; n = 8) (Fig. 10A). The $\delta^{18}O$ values of pure HCD and LCD are not correlated with the %Ca (Fig. 10B–D) with the $\delta^{13}C$ values of pure HCD (1.5–2.7 ‰, average 2.8 ‰; n = 39) being similar to those of the pure LCD (2.0–2.7 ‰, average 2.5 ‰; n = 8) (Fig. 10A) (Supplementary-Table 1).

Based on 99 samples, the Mn/Sr ratios of the dolostones range from 0.1 to 0.9 (average 0.2), the Fe content ranges from 118 to 1077 ppm (average 435 ppm), and the Mn content ranges from 10 to 254 ppm (average 54 ppm) (Fig. 2F–H). There are no systematic variations in Mn/Sr, Fe, or Mn contents through the Huangliu Formation (Fig. 2F–H). The Fe content of pure HCD (118–1077 ppm; average 438 ppm; n = 38) is similar to that of pure LCD (126–852 ppm; average 423 ppm; n = 8) (Fig. 10E). The Mn content in pure HCD (12–234 ppm; average 57 ppm; n = 38) is characterized by a slight larger range of values and a higher average value relative to that in pure LCD (11–71 ppm; average 39 ppm; n = 8) (Fig. 10F) (Supplementary-Table 1).

5. Comparison with dolostones from Grand Cayman

Although located 15,795 km apart, the dolostones of the Cayman Formation (Miocene) on Grand Cayman (Caribbean Sea) are remarkably similar to the dolostones in the Huangliu Formation on Chenhang Dao (South China Sea). The dolostones of Cayman Formation have been well-characterized by Jones et al. (2001), Jones and Luth (2002), and Ren and Jones (2017, 2018).

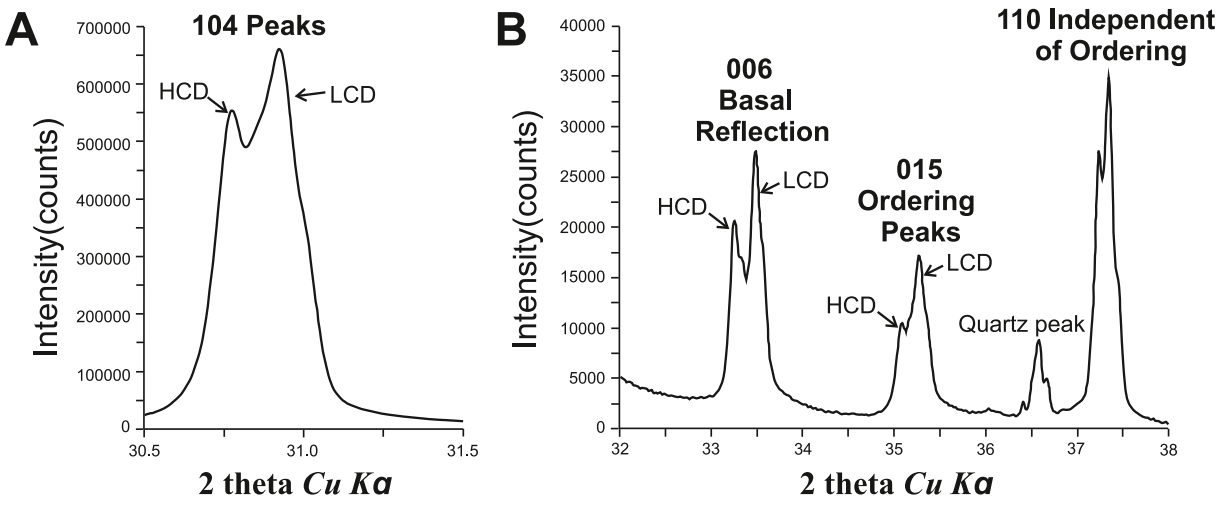

Fig. 6. Segments of XRD diffractogram for a dolostone (489 m bsl) from the Huangliu Formation of well CK-2 in the Xisha Islands. Quartz is added as an internal standard. (A) Overlapping 104 peaks of LCD and HCD. (B) Double basal reflection (006) and ordering peaks (015) that correspond to the LCD and HCD peaks shown in A. The 110 peak is independent of ordering.

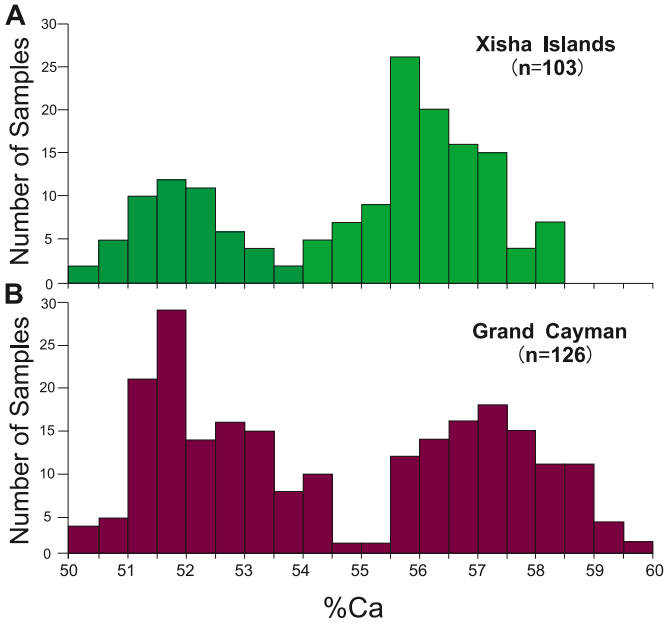

Fig. 7. Bimodal frequency distribution of %Ca in the dolomites from the (A) Huangliu Formation in the Xisha Islands, and (B) Cayman Formation from Grand Cayman (data from Jones and Luth, 2002).

5.1. Geological setting

Grand Cayman, ~35 km long and 6–14 km wide, is located south of Cuba and northwest of Jamaica. The Bluff Group, which forms the upper part of the carbonate succession is divided into the unconformity-bounded Brac Formation (late Oligocene), Cayman Formation (early to middle Miocene), and Pedro Castle Formation (Pliocene). The Ironshore Formation (Pleistocene) unconformably overlies the Bluff Group (e.g. Jones et al., 1994a,b). The Brac Formation and the Pedro Castle Formation are typically formed of limestones and dolostones, whereas the Cayman Formation is formed largely of dolostones (Jones et al., 1994a, b; Zhao and Jones, 2012). Grand Cayman appears to have experienced little, if any, tectonic movements since the Oligocene (e.g., Jones and Hunter, 1990; Vézina et al., 1999; Coyne et al., 2007).

5.2. Comparison of dolostone successions

Today, dolostones in the Cayman Formation are between ~160 m bsl and ~40 m above sea level (asl). In contrast, dolostones in the Huangliu Formation are ~300–520 m below sea level (bsl). This contrast in depths reflects the fact that the Cayman Formation has experienced significantly less tectonic subsidence than the Huangliu Formation (Wang et al., 2019). The remarkable similarities between the dolostone in the Huangliu Formation and the Cayman Formation are highlighted by the following: (1) original sediments that formed in shallow marine waters (< 30 m); (2) unconformities that form the lower and upper boundaries of both formations; (3) karst development that occurred in conjunction with the development of the unconformities at the top of both formations; (4) dolomitization that took place during the late Miocene to early Pleistocene; (5) the petrography of the dolostones in both formations.

5.3. Dolomite stoichiometry

Dolostones in the Cayman Formation are formed of LCD and HCD (Fig. 3; Fig. 5E and F). Backscatter images of dolomite crystals from this formation show numerous crystals with HCD cores encased by LCD or by alternating zones (1–10 μm thick) of LCD and HCD (Fig. 5E and F). The alternating HCD and LCD zones are more common than in the Huangliu Formation (Fig. 5). Dolostones in the Cayman Formation, like those in the Huangliu Formation, are composed of 100 % LCD, 100 % HCD, or a mixture of LCD and HCD (e.g., well LV#2 – Fig. 3). In the Cayman Formation, there is no obvious correlation between the %LCD and % HCD with depth (Fig. 3). There is a consistent difference between the LCD and HCD of ~5 %Ca (Fig. 5E and F; Fig. 8B), which is akin to that in the dolomite crystals in the Huangliu Formation (Fig. 5B–D; Fig. 8A). On Grand Cayman, the percentage of LCD and the %Ca content of the dolomite generally decreases from the coastal dolostones to the interior limestone and dolostone (Ren and Jones, 2017).

5.4. Division between LCD and HCD

For the dolostones from the Cayman Formation on Grand Cayman, Jones and Luth (2002) placed the division between the LCD and HCD at 55 %Ca (Fig. 7B). Based on the %Ca frequency histogram for dolomite from the Huangliu Formation, it could be argued that the division between HCD and LCD should be placed at ~54 %Ca (Fig. 7A). This would mean, however, that the division between LCD and HCD can vary from locality to locality. This option would cause considerable confusion

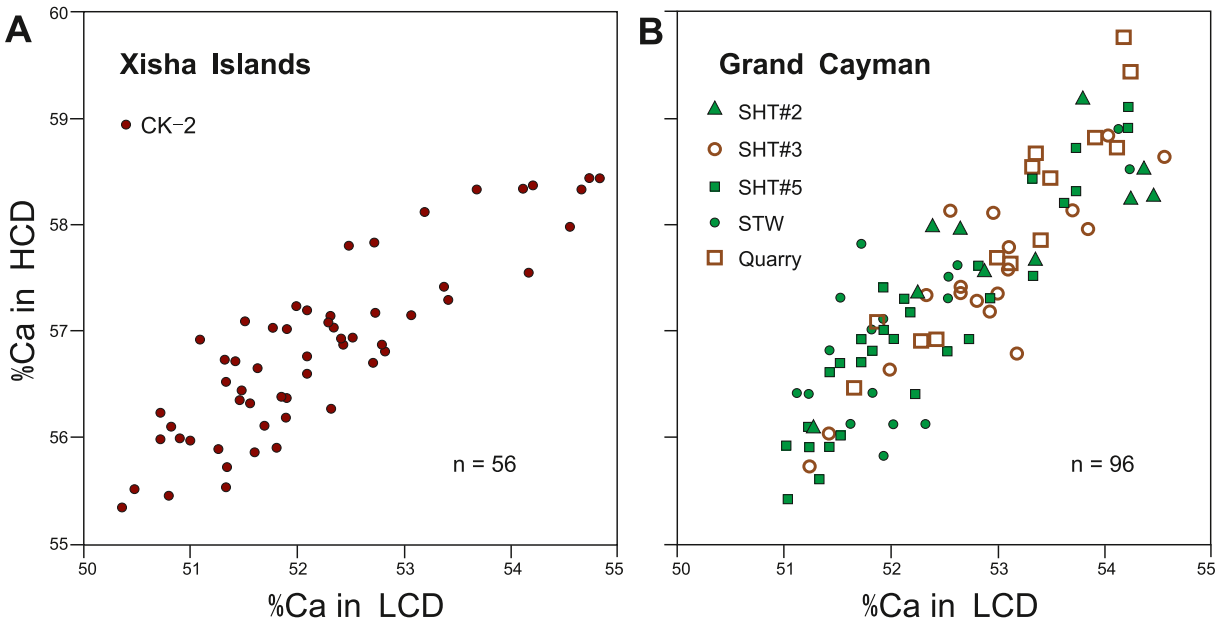

Fig. 8. Bivariant graphs showing high correlation between %Ca in LCD and HCD from the (A) Huangliu Formation, Xisha Islands and (B) Cayman Formation, Grand Cayman (data from Jones and Luth, 2002). Note constant difference between %Ca in HCD and LCD of ~4.5 % for the Huangliu Formation and ~5 % for the Cayman Formation.

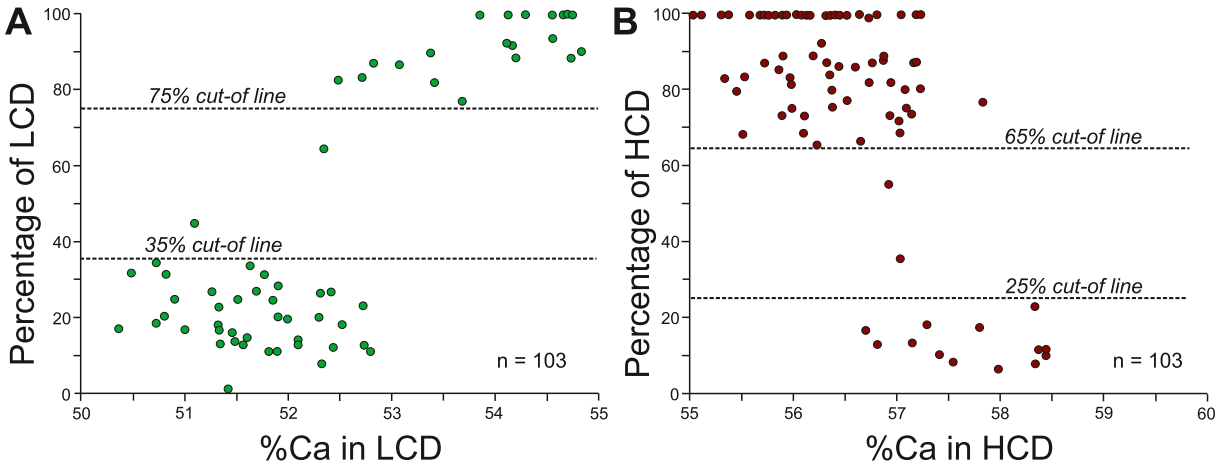

Fig. 9. Cross plot of the %Ca in LCD and HCD with the %LCD and %HCD (percentage of LCD and HCD respectively) in Huangliu Formation from well CK-2 in the Xisha Islands.

because the definition of LCD and HCD would vary from locality to locality. Accordingly, the division between LCD and HCD is herein kept at 55 %Ca, as defined by Jones and Luth (2002).

6. Discussion

6.1. Coexistence of LCD and HCD as primary growth features in dolostones

From a thermodynamic perspective, high-calcium dolomites (HCD) are inherently unstable and prone to transformation into low-calcium dolomite (LCD) during recrystallization (Chilingar, 1956; Land, 1980; Lumsden and Chimahusky, 1980; Sperber et al., 1984). Many high-temperature (most > 175 °C) experiments have also shown that stoichiometric dolomite develops through a series of metastable precursors that progresses through high-Mg calcite, very high-Mg calcite (VHMC), to nonstoichiometric, poorly ordered dolomite (e.g., Katz and Matthews, 1977; Sibley, 1990; Sibley et al., 1994; Kaczmarek and Sibley, 2011, 2014). Accordingly, the coexistence of HCD and LCD in most ancient dolomites/dolostones has generally been attributed to recrystallization that took place during burial (e.g. Woronick and Land, 1985; Kupecz et al., 1994; Olanipekun and Azmy, 2017; Guo et al., 2020). Nevertheless, dolostones formed of two or more compositional populations, as defined by their %Ca, are common in many Tertiary island dolostones, including those on Niue, the Great Bahama Bank, and Kita-daito-jima (Wheeler et al., 1999; Swart and Melim, 2000; Suzuki et al., 2006) that have not experience significant burial.

The bimodal %Ca compositions evident in the island dolostones of the Huangliu Formation (Fig. 7A) and Cayman Formation (Fig. 7B) clearly shows that the presence of two dolomite populations is not a local phenomenon. Backscatter imaging shows that many dolomite crystals in those two formations are characterized of HCD cores encased by LCD or alternating LCD and HCD zones, 1–10 μm wide, that are separated by sharp boundaries (Fig. 5B–F). Wang et al. (2018) argued that such zoning coupled with the cathodoluminescence and geochemical characteristics showed that the dolostones in the Huangliu

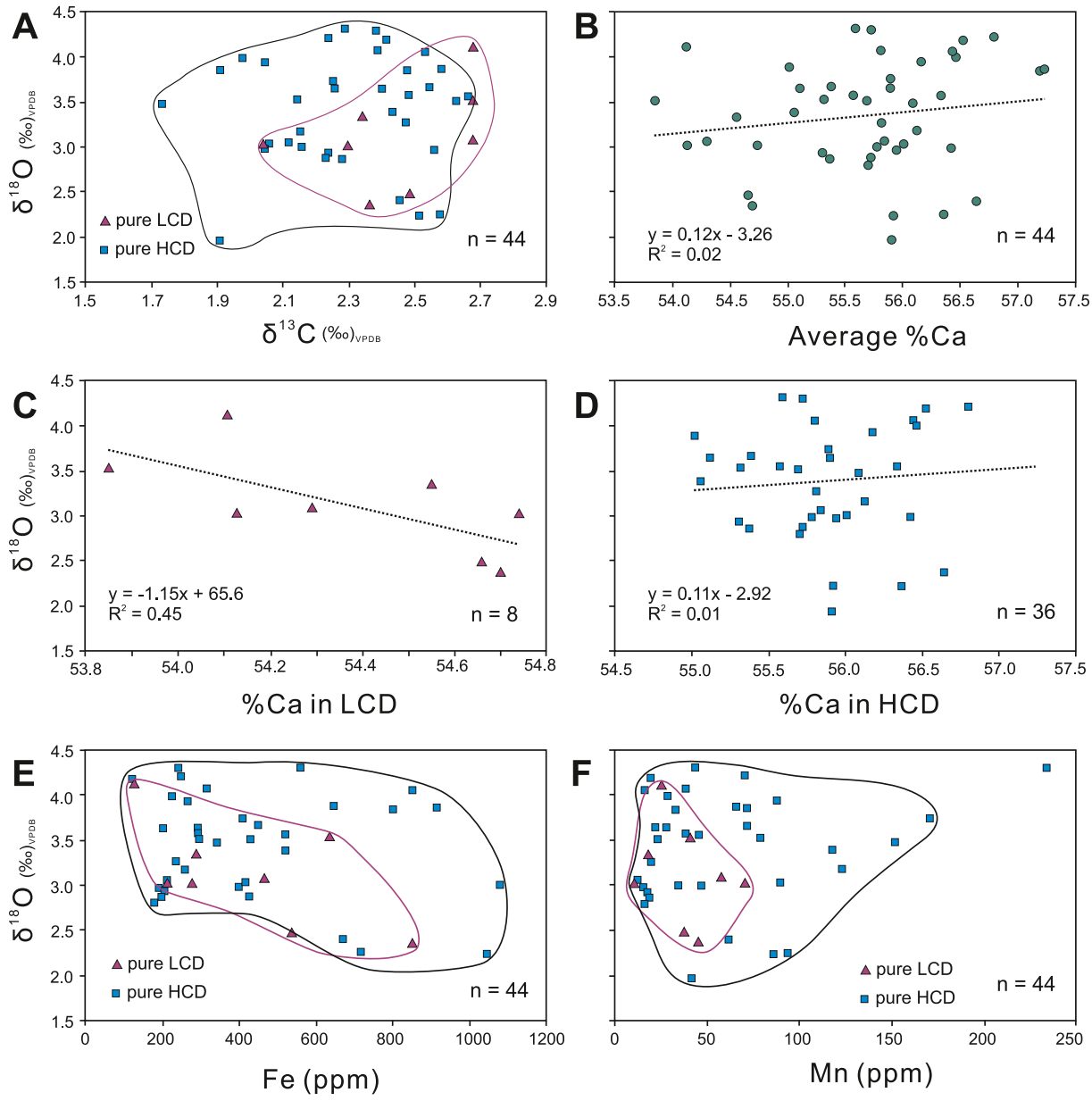

Fig. 10. Bivariant graphs showing various geochemistry properties from the dolomites of Huangliu Formation of well CK-2 in the Xisha Islands. A) $\delta^{13}C$ versus $\delta^{18}O$ of pure LCD and HCD. B) $\delta^{18}O$ versus average %Ca with calculated regression axis. C) $\delta^{18}O$ versus %Ca in pure LCD with calculated regression axis. D) $\delta^{18}O$ versus % Ca in pure HCD with calculated regression axis. E) Fe contents of pure LCD and HCD. F) Mn contents of pure LCD and HCD.

Formation had not been modified by recrystallization. Similar conclusions have been reached for the dolostones in the Cayman Formation on Grand Cayman (Jones and Luth, 2002; Ren and Jones, 2017). Kaufman and Knoll (1995) suggested that an increase in Mn content coupled with a decrease in Sr content can be used to evaluate the degree of diagenesis. Thus, Jacobsen and Kaufman, 1999 and Dehler et al. (2005) suggested that carbonates with Mn/Sr $<$ 2 and Mn/Sr $<$ 3, respectively, have undergone little or no diagenesis. The low Mn/Sr ratios (0.1–0.9, average = 0.2, n = 99) in the dolostones of the Huangliu Formation (Fig. 2H) indicate that diagenetic alteration since dolomitization has been minimal. Collectively, these facts indicate that the dolostones in the Huangliu Formation and Cayman Formation exhibit primary features with little to no post-dolomitization modifications.

The coexistence of LCD and HCD in the dolomite crystals from the Huangliu Formation and Cayman Formation shows that conditions leading to the growth of dolomite crystals varied on a microscale. As suggested by Jones and Luth (2002), alternating HCD and LCD zones in the dolomite crystals of the Cayman Formation are akin to oscillatory zoning (cf., Shore and Fowler, 1996). Such zoning, also evident in dolomite crystals in the Huangliu Formation, is a common phenomenon in many minerals (Shore and Fowler, 1996) that may be controlled by intrinsic factors such as growth inhibitor adsorption and/or extrinsic factors such as fluid composition, temperature, salinity, or alkalinity (e.g., Shore and Fowler, 1996; Reeder et al., 1990).

6.2. Formation of LCD and HCD

Dolomitization is generally considered to be a dissolution – reprecipitation phenomenon that involves dissolution, transportation of ions, and precipitation (e.g., Katz and Matthews, 1977; Veizer, 1983; Putnis and John, 2010; Mueller et al., 2010; Jonas et al., 2015). Previous studies have shown that the chemical composition of the dolomite is kinetically controlled and determined by the composition of the fluid that mediates the reaction (e.g., Rosenberg et al., 1967; Sibley, 1990;

Tribble et al., 1995; Kaczmarek and Sibley, 2007, 2011; 2014; Jonas et al., 2015). The complex array of factors that control dolomite stoichiometry in high-temperature experiments include precursor mineralogy (aragonite versus calcite), surface area, crystal size of the reactants, alkalinity, Mg and Ca concentrations, salinity, temperature and pCO_2 of the fluids, and/or the water-rock ratio (e.g. Katz and Matthews, 1977; Baker and Kastner, 1981; Bullen and Sibley, 1984; Sibley et al., 1987; Sibley et al., 1994; Land, 1998; Arvidson and McKenzie, 1999; Gregg et al., 2015). Despite this plethora of possible factors, most discussions regarding dolomitization have focused largely on the Mg/Ca ratios (Sibley et al., 1987; Kaczmarek and Sibley, 2011), temperature (Kaczmarek and Thornton, 2017), and/or salinity (Cohen and Kaczmarek, 2018).

Variation in the $\delta^{18}O$ of dolostones may reflect changes in the isotopic composition of water, temperature, and other factors such as dolomite stoichiometry (Vahrenkamp and Swart, 1994; Budd, 1997; Swart, 2015). Dolomite with high %Ca generally have isotopically lighter oxygen isotopic compositions than true stoichiometric dolomite (50:50 Mg:Ca ratios) due to the influence of varying strengths in the Mg–O and Ca–O bonds (e.g., Budd, 1997; Gregg et al., 2015). Theoretically, the oxygen isotopic composition ($\delta^{18}O$) of dolomite can increase from 0.06 to 0.12‰ with every 1 % increase in the mole % $MgCO_3$ (Tarutani et al., 1969; Land, 1980). For the dolostones in the Huangliu Formation, however, it does not appear that the $\delta^{18}O$ values are linked to the %Ca of the dolomite given that the $\delta^{18}O$ values tend to increase as the average %Ca increases (Fig. 10B–D). The similar range of $\delta^{18}O$ values for the pure HCD (1.9–4.3 ‰; n = 39) and pure LCD (2.4–4.1 ‰; n = 8) (Fig. 10A) also argues against dolomite stoichiometry being correlated with the $\delta^{18}O$ values. It appears, therefore, that the $\delta^{18}O$ in the HCD and/or LCD was influenced by the properties of dolomitization fluids (e.g. ^{18}O composition, temperature). Many studies from field and laboratory observations also suggest that dolomite stoichiometry may reflect the properties of the dolomitizing fluids (Lumsden and Chimahusky, 1980; Kaczmarek and Sibley, 2011; Ren and Jones, 2017; Manche and Kaczmarek, 2019). The range of $\delta^{18}O$ values for the HCD and LCD in the Huangliu Formation, which is similar to the 0.5–4.5 ‰ range recorded from many island dolomites (e.g., Budd, 1997; Ren and Jones, 2018), suggests that dolomite precipitation was mediated by normal or slightly modified seawater.

In the Huangliu Formation, the difference in the %Ca content between samples with a high %LCD content and a high %HCD content (Fig. 9A and B) should indicate that the formation of LCD and HCD was influenced by fluids with different properties. From a thermodynamic perspective, dolomite with a high %Ca content forms at temperatures <200 °C (e.g., Arvidson and Mackenzie, 1999). Conversely, kinetic precepts suggest that solutions with high Mg/Ca ratios, high temperatures, and high salinity should lead to faster rates of dolomitization and lower %Ca dolomite (e.g., Kaczmarek and Sibley, 2011; Kaczmarek and Thornton, 2017; Cohen and Kaczmarek, 2018). The interaction between thermodynamic and kinetic factors can therefore lead to two extreme situations. (1) If the physicochemical parameters of the dolomitization fluids (e.g., elevated Mg/Ca, salinity, temperature) enhance the kinetics of dolomitization, then LCD should be the dominant type of dolomite (Fig. 9A) (Kaczmarek and Sibley, 2011; Kaczmarek and Thornton, 2017; Cohen and Kaczmarek, 2018). (2) If the physicochemical conditions of the dolomitization fluids (e.g., Mg/Ca, salinity, temperature) not enhancing the kinetics, then HCD should dominate (Fig. 9B) (Kaczmarek and Sibley, 2011; Kaczmarek and Thornton, 2017; Cohen and Kaczmarek, 2018).

For the Huangliu Formation, the dominance of samples formed largely of LCD or HCD and the rarity of intermediate compositions (2 of 103 samples) suggests that two end members of the dolomitization kinetics were operative with variants between them being rare (Fig. 9). This notion is supported by the sharp boundaries between the LCD and HCD zones (Fig. 5B–F), which indicate that conditions oscillated between two end members without any gradual changes being involved. For the Huangliu Formation, it seems that the LCD probably formed under more enhanced kinetic factors than the HCD – a notion that is consistent with the observation derived from high temperature experiments (Kaczmarek and Sibley, 2011; Kaczmarek and Thornton, 2017; Cohen and Kaczmarek, 2018).

The Fe contents in the HCD (118–1077 ppm; average 438 ppm) and LCD (126–852 ppm; average 423 ppm) and Mn contents of the HCD (12–234 ppm; average 57 ppm) and LCD (11–71 ppm; average 39 ppm) in the Huangliu Formation (Fig. 10E and F) are similar to those found in many island dolomites, including those from the Little Bahama Bank and Midway Atoll (Budd, 1997). Such comparisons indicate that the redox state of the dolomitizing fluids had little influence on formation of the HCD and LCD.

The high correlation between the %Ca in the LCD and %Ca in the HCD in the dolostones of the Huangliu Formation (Fig. 8A) and Cayman Formation (Fig. 8B) suggests that the Mg was incorporated into the dolomite by similar processes that were independent of location. The similarity in the difference in %Ca between HCD and LCD layers, typically ~5 %Ca, in the dolomite crystals (Fig. 5B–D) suggests that the incorporation of Mg may have been influenced by crystal structure. Searl (1994) argued that the composition of a compositional zone in a crystal might influence the composition of the succeeding layer. Fouke and Reeder (1992) also suggested that the incorporation of Mg or Ca ions on dolomite crystal surfaces during growth was controlled, at least in part, by their adsorption density. Thus, it is possible that this phenomenon may have played an important role in the incorporation of Mg into the dolomite crystal. This phenomenon is also evident from high-T experiments given that the composition of the dolomite remains constant during most of the reaction even though the Mg/Ca ratio in the solution continually evolves as Mg is captured by the growing dolomite crystal and Ca is released from the calcite into solution (Kaczmarek and Sibley, 2011).

6.3. Microenvironments controlling the development of dolomite crystal

The formation of island dolostones has been variously attributed to tidal pumping, reflux, mixing of seawater and freshwater, ocean current pumping, and/or Kohout convection (e.g., Tucker and Wright, 1990; Budd, 1997; Ren and Jones, 2018). All of these models tacitly imply that dolomitization is controlled primarily by large-scale factors, such as temperature, salinity, Mg/Ca ratios, and pCO_2 that influence the composition of the fluids and fluid movement (e.g. Morrow, 1982a; Land, 1985; Machel, 2004). It is difficult, however, to relate those large scales, island-wide factors to the development of individual dolomite crystals with variable HCD and LCD contents.

In the Huangliu Formation and the Cayman Formation there is no obvious correlation between depth and the %Ca in LCD, %Ca in HCD, or average %Ca (Figs. 2 and 3). In the Cayman Formation on Grand Cayman, dolomite stoichiometry also varies laterally, so that neighboring wells only 100–150 m apart (e.g., STW and SHT#3) (Jones and Luth, 2002, their Figs. 6 and 9) have obvious differences in the stratigraphic trends of their %Ca in LCD, %Ca in HCD, and average %Ca. Available evidence from both formations indicates that the fluids that mediated formation of the HCD and LCD varied laterally and vertically throughout the successions. Ren and Jones (2017, 2018) suggested that on many islands, the degree of dolomitization and the %HCD and %Ca of the dolostones may vary laterally because of changes in the water-rock interaction along the flow path of the dolomitization fluid (e.g., seawater) as it moves from the shelf edge to the island center. Thus, the variation of fluid properties, at all scales, will determine the growth of individual dolomite crystals and the temporal alternation between HCD and LCD. The higher number of HCD and LCD zones in the dolomite crystals of the Cayman Formation compared to those in the Huangliu Formation (Fig. 5) may indicate that micro-environmental conditions were more variable on Grand Cayman than on Chenhang Island. In addition, in unit 2 of the Huangliu Formation, the relationship between

the average %Ca, the $\delta^{18}O$, the percentage of HCD and LCD and depth (Fig. 2B–E) indicates that the dolomitization fluids that controlled dolomite stoichiometry were, to some extent, influenced by the sedimentary environment or water depth. Manche and Kaczmarek (2019) also argued that vertical variations in dolomite stoichiometry are related to changes in the depositional environment/water depth.

The similarities between the dolostones in Huangliu Formation and Cayman Formation suggests that dolomitization conditions on Grand Cayman and the Xisha Islands were similar – even though they are located in different oceans thousands of kilometers apart. Development of the dolostones in the Huangliu Formation and Cayman Formation during the late Miocene to early Pleistocene (~10–2.5 Ma) (Wang et al., 2018a; Ren and Jones, 2017, 2018) took place while both successions were located in open seas in tropical regions that experienced similar seawater properties (e.g. Mg/Ca ratios, salinity, temperature), global climate factors such as gradually cooling and drying weather (Zachos et al., 2001), high atmospheric pCO_2 (from 454 to 250 ppmv between ~11 and 6 Ma) (Mejía et al., 2017), and fluctuating sea levels (~−100 to +100 m) (Haq et al., 1987). These large-scale factors, which would determine the large-environmental backgrounds of the Xisha Islands and Cayman Islands, should provide general controls on the island dolomitization process. It is also critically important, however, to consider the micro-scale conditions, especially while the water-reaction occurred during the fluids flow through the islands. Scale is a critical aspect because the large-scale factors controlled the composition and pattern of the circulating groundwaters but the growth and development of individual crystals are controlled by microenvironmental conditions. This dichotomy in scale is a critical issue that has not been addressed in the dolomitization models that have been invoked to explain the development of island dolomite.

7. Conclusions

Through the comparison of Miocene dolostones from Xisha Islands (South China Sea) and the dolostones from Grand Cayman (Caribbean Sea), we reveal the high similarity in the features of dolomite stoichiometry between them. LCD and HCD, as defined by the %Ca in these island dolostones, are primary growth features (no obvious recrystallization) that formed as the dolomite replaced the limestone precursor. The LCD seems to have formed under more enhanced kinetic factors (e.g., elevated high temperature, salinity, Mg/Ca ratios) than the HCD, although the LCD and HCD were both mediated by normal or slightly modified seawater. The variation of fluid properties at micro-scale fundamentally determines the growth of individual dolomite crystals and the temporal alternation between HCD and LCD. For a better understanding the full range of dolomitization processes, this study suggests that any dolomitization model proposed for the development of island dolostones should include the large-scale factors that promoted dolomitization and the micro-scale conditions that controlled the growth of the constituent crystals.

Declaration of competing interest

The authors declare that they have no known competing financial interests or personal relationships that could have appeared to influence the work reported in this paper.

Acknowledgement

This work was funded by the National Natural Science Foundation of China, China (Nos. 42030502, 42090041 and 41962010), Science and Technology Major Project of Guangxi, China (Nos. AD17129063 and AA17204074), and Natural Science Foundation of Guangxi Province, China (2017GXNSFBA198242). We thank to the drilling crews from the Guizhou Bureau of Geology and Mineral Resources, and numerous staff members from the South China Sea Institute of Oceanology and Wuhan Institute of Rock and Soil Mechanics, Chinese Academy of Sciences, who helped to collect samples during drilling.

Appendix A. Supplementary data

Supplementary data to this article can be found online at https://doi.org/10.1016/j.marpetgeo.2021.105286.

Credit author statement

Rui Wang: Testing XRD and observing the core, providing original draft preparation, writing and revising papers, Kefu Yu: Collecting samples, providing original draft preparation, Brian Jones: Editing the language, writing and revising the papers, Wei Jiang: Collecting samples, testing the elements, Shendong Xu: Collecting samples, grinding, testing the C/O isotopes, Tianlai Fan: Collecting samples, giving advice for the manuscript, Yu Zhang: Collecting samples, giving advice for the manuscript.

References

Arvidson, R.S., Mackenzie, F.T., 1999. The dolomite problem; control of precipitation kinetics by temperature and saturation state. Am. J. Sci. 299, 257–288.
Baker, P.A., Kastner, M., 1981. Constraints on the formation of sedimentary dolomite. Science 213, 214–216.
Bi, D., Zhai, S., Zhang, D., Liu, X., Liu, X., Jiang, L., Zhang, A., 2018. Constraints of fluid inclusions and C, O isotopic compositions on the origin of the dolomites in the Xisha Islands, South China Sea. Chem. Geol. 493, 504–517.
Budd, D.A., 1997. Cenozoic dolomites of carbonate islands: their attributes and origin. Earth Sci. Rev. 42, 1–47.
Bullen, S.B., Sibley, D.F., 1984. Dolomite selectivity and mimic replacement. Geology 12, 285–287.
Chilingar, G.V., 1956. Relationship between Ca/Mg ratio and geologic age. AAPG Bull. 40, 2256–2266.
Cohen, H.F., Kaczmarek, S.E., 2018. Evaluating the Effects of Fluid Chemistry on Dolomite Stoichiometry and Reaction Rate. AAPG ACE 2018 Annual Convention & Exhibition.
Coyne, M.K., Jones, B., Ford, D., 2007. Highstands during marine isotope stage 5: evidence from the Ironshore Formation of Grand cayman, British west indies. Quat. Sci. Rev. 26, 536–559.
Dehler, C., Elrick, M., Bloch, J., Crossey, L., Karlstrom, K., Marais, D.D., 2005. High-resolution $\delta^{13}C$ stratigraphy of the Chuar Group (ca. 770–742 Ma), Grand Canyon: implications for mid-Neoproterozoic climate change. Geol. Soc. Am. Bull. 117, 32–45.
Dunham, R.J., 1962. Classification of carbonate rocks according to depositional texture. AAPG Mem 1, 108–121.
Fan, T., Yu, K., Zhao, J., Jiang, W., Xu, S., Zhang, Y., Wang, R., Wang, Y., Feng, Y., Bian, L., 2020. Strontium isotope stratigraphy and paleomagnetic age constraints on the evolution history of coral reef islands, northern South China Sea. Geol. Soc. Am. Bull. 132, 803–816.
Fouke, B.W., Reeder, R.J., 1992. Surface structural controls on dolomite composition: evidence from sectoral zoning. Geochem. Cosmochim. Acta 56, 4015–4024.
Given, R.K., Wilkinson, B.H., 1987. Dolomite abundance and stratigraphic age: constraints on rates and mechanisms of Phanerozoic dolostone formation. J. Sediment. Res. 57, 1068–1078.
Gregg, J.M., Bish, D.L., Kaczmarek, S.E., Machel, H.G., Hollis, C., 2015. Mineralogy, nucleation and growth of dolomite in the laboratory and sedimentary environment: a review. Sedimentology 62, 1749–1769.
Guo, C., Chen, D., Qing, H., Zhou, X., Ding, Y., 2020. Early dolomitization and recrystallization of the lower-middle ordovician carbonates in western tarim basin (NW China). Mar. Petrol. Geol. 111, 332–349.
Haq, B.U., Hardenbol, J., Vail, P.R., 1987. Chronology of fluctuating sea levels since the Triassic. Science 235, 1156–1167.
Jacobsen, S.B., Kaufman, A.J., 1999. The Sr, C and O isotopic evolution of Neoproterozoic seawater. Chem. Geol. 161, 37–57.
Jiang, W., Yu, K., Fan, T., Xu, S., Wang, R., Zhang, Y., Yue, Y., Zhao, J., Feng, Y., Wei, C., 2019. Coral reef carbonate record of the Pliocene-Pleistocene climate transition from an atoll in the South China Sea. Mar. Geol. 411, 88–97.
Jonas, L., Müller, T., Dohmen, R., Baumgartner, L., Putlitz, B., 2015. Transport-controlled hydrothermal replacement of calcite by Mg-carbonates. Geology 43, 779–782.
Jones, B., Hunter, I., 1990. Pleistocene paleogeography and sea levels on the Cayman Islands, British West Indies. Coral Reefs 9, 81–91.
Jones, B., Hunter, I., Kyser, K., 1994a. Revised stratigraphic nomenclature for tertiary strata of the Cayman Islands, British west indies. Caribb. J. Sci. 30, 53–68.
Jones, B., Hunter, I., Kyser, K., 1994b. Stratigraphy of the Bluff formation (Miocene-Pliocene) and the newly defined Brac Formation (Oligocene), cayman brac, British west indies. Caribb. J. Sci. 30, 30–51.
Jones, B., Luth, R.W., 2002. Dolostones from Grand cayman, British west indies. J. Sediment. Res. 72, 559–569.

Jones, B., Luth, R.W., MacNeil, A.J., 2001. Powder X-ray diffraction analysis of homogeneous and heterogeneous sedimentary dolostones. J. Sediment. Res. 71, 790–799.
Kaczmarek, S.E., Sibley, D.F., 2007. A comparison of nanometer-scale growth and dissolution features on natural and synthetic dolomite crystals: implications for the origin of dolomite. J. Sediment. Res. 77, 424–432.
Kaczmarek, S.E., Sibley, D.F., 2011. On the evolution of dolomite stoichiometry and cation order during high-temperature synthesis experiments: an alternative model for the geochemical evolution of natural dolomites. Sediment. Geol. 240, 30–40.
Kaczmarek, S.E., Sibley, D.F., 2014. Direct physical evidence of dolomite recrystallization. Sedimentology 61, 1862–1882.
Kaczmarek, S.E., Thornton, B.P., 2017. The effect of temperature on stoichiometry, cation ordering, and reaction rate in high-temperature dolomitization experiments. Chem. Geol. 468, 32–41.
Kaczmarek, S.E., Gregg, J.M., Bish, D.L., Machel, H.G., Fouke, B.W., 2017. Dolomite, very high-magnesium calcite, and microbes - implications for the microbial model of dolomitization. In: MacNeil, A., Lonnee, J., Wood, R. (Eds.), Characterization and Modeling of Carbonates— Mountjoy Symposium 1, vol. 109. Society for Sedimentary Geology (SEPM) Spec. Publ, pp. 7–20.
Katz, A., Matthews, A., 1977. The dolomitization of $CaCO_3$: an experimental study at 252-295°C. Geochem. Cosmochim. Acta 41, 297–308.
Kaufman, A.J., Knoll, A.H., 1995. Neoproterozoic variations in the C-isotopic composition of seawater: stratigraphic and biogeochemical implications. Precambrian Res. 73, 27–49.
Kupecz, J.A., Land, L.S., Purser, B., Tucker, M., Zenger, D., 1994. Progressive recrystallization and stabilization of early-stage dolomite: lower Ordovician Ellenburger Group, west Texas. In: Purser, B., Tucker, M., Zenger, D. (Eds.), Dolomites: A Volume in Honour of Dolomieu, vol. 21. International Association of Sedimentologists Spec. Publ., pp. 255–279
Land, L.S., 1980. The isotopic and trace element geochemistry of dolomite: the state of the art. In: Zenger, D.H., Dunham, J.B., Ethington, R.L. (Eds.), Concepts and Models of Dolomitization, vol. 28. SEPM Spec. Publ., pp. 87–110
Land, L.S., 1985. The origin of massive dolomite. J. Geol. Educ. 33, 112–125.
Land, L.S., 1998. Failure to precipitate dolomite at 25°C from dilute solution despite 1000-Fold oversaturation after 32 years. Aquat. Geochem. 4, 361–368.
Lumsden, D.N., 1979. Discrepancy between thin-section and X-ray estimates of dolomite in limestone. J. Sediment. Res. 49, 429–435.
Lumsden, D.N., Chimahusky, J.S., 1980. Relationship between dolomite nonstoichiometry and carbonate facies parameters. In: Zenger, D.H., Dunham, J.B., Etherington, R.L. (Eds.), Concepts and Models of Dolomitization, vol. 28. SEPM Spec. Publ., pp. 123–138
Machel, H.G., 2004. Concepts and models of dolomitization: a critical reappraisal. In: Braithwaite, C.J.R., Rizzi, G., Darke, G. (Eds.), The Geometry and Petrogenesis of Dolomite Hydrocarbon Reservoirs, vol. 245. Geol. Soc. London, Spec. Publ., pp. 7–63
Manche, C.J., Kaczmarek, S.E., 2019. Evaluating reflux dolomitization using a novel high-resolution record of dolomite stoichiometry: a case study from the Cretaceous of central Texas, USA. Geology 47, 586–590.
Mckenzie, J.A., Vasconcelos, C., 2009. Dolomite Mountains and the origin of the dolomite rock of which they mainly consist: historical developments and new perspectives. Sedimentology 56, 205–219.
Mejía, L.M., Méndez-Vicente, A., Abrevaya, L., Lawrence, K.T., Ladlow, C., Bolton, C., Cacho, I., Stoll, H., 2017. A diatom record of CO_2 decline since the late Miocene. Earth Planet Sci. Lett. 479, 18–33.
Morrow, D., 1982a. Diagenesis 1. Dolomite-Part 1: the chemistry of dolomitization and dolomite precipitation. Geosci. Can. 9, 5–13.
Morrow, D., 1982b. Diagenesis 2. Dolomite-Part 2 Dolomitization models and ancient dolostones. Geosci. Can. 9, 95–107.
Mueller, T., Watson, E.B., Harrison, T.M., 2010. Applications of diffusion data to high-temperature earth systems. Rev. Mineral. Geochem. 72, 997–1038.
Olanipekun, B.J., Azmy, Karem, 2017. In situ characterization of dolomite crystals: evaluation of dolomitization process and its effect on zoning. Sedimentology 64, 1708–1730.
Petrash, D.A., Bialik, O.M., Bontognali, T.R., Vasconcelos, C., Roberts, J.A., McKenzie, J. A., Konhauser, K.O., 2017. Microbially catalyzed dolomite formation: from near-surface to burial. Earth Sci. Rev. 171, 558–582.
Putnis, A., John, T., 2010. Replacement processes in the Earth's crust. Elements 6, 159–164.
Reeder, R.J., Fagioli, R.O., Meyers, W.J., 1990. Oscillatory zoning of Mn in solution-grown calcite crystals. Earth Sci. Rev. 29, 39–46.
Ren, M., Jones, B., 2017. Spatial variations in the stoichiometry and geochemistry of Miocene dolomite from Grand Cayman: implications for the origin of island dolostone. Sediment. Geol. 348, 69–93.
Ren, M., Jones, B., 2018. Genesis of island dolostones. Sedimentology 65, 2003–2033.
Rosenberg, P., Burt, D., Holland, H., 1967. Calcite-dolomite-magnesite stability relations in solutions: the effect of ionic strength. Geochem. Cosmochim. Acta 31, 391–396.
Searl, A., 1994. Discontinuous solid solution in Ca-rich dolomites: the evidence and implications for the interpretation of dolomite petrographic and geochemical data. In: Purser, B., Tucker, M., Zenger, D. (Eds.), Dolomites. A Volume in Honour of Dolomieu, vol. 21. Int. Assoc. Sedimento. Spec. Publ., pp. 361–376
Shao, L., Cui, Y., Qiao, P., Zhang, D., Liu, X., Zhang, C., 2017a. sea-level changes and carbonate platform evolution of the Xisha islands (south China sea) since the early Miocene. Palaeogeogr. Palaeoclimatol. Palaeoecol. 485, 504–516.
Shao, L., Li, Q., Zhu, W., Zhang, D., Qiao, P., Liu, X., You, L., Cui, Y., Dong, X., 2017b. Neogene carbonate platform development in the NW South China Sea: litho-, bio- and chemo-stratigraphic evidence. Mar. Geol. 385, 233–243.
Shore, M., Fowler, A.D., 1996. Oscillatory zoning in minerals: a common phenomenon. Can. Mineral. 34, 1111–1126.
Sibley, D.F., 1990. Unstable to stable transformations during Dolomitization. J. Geol. 98, 739–748.
Sibley, D.F., Dedoes, R.E., Bartlett, T.R., 1987. Kinetics of dolomitization. Geology 15, 1112–1114.
Sibley, D.F., Nordeng, S.H., Borkowski, M.L., 1994. Dolomitization kinetics of hydrothermal bombs and natural settings. J. Sediment. Res. 64, 630–637.
Sperber, C.M., Wilkinson, B.H., Peacor, D.R., 1984. Rock composition, dolomite stoichiometry, and rock/water reactions in dolomitic carbonate rocks. J. Geol. 92, 609–622.
Suzuki, Y., Iryu, Y., Inagaki, S., Yamada, T., Aizawa, S., Budd, D.A., 2006. Origin of atoll dolomites distinguished by geochemistry and crystal chemistry: Kita-daito-jima, northern Philippine Sea. Sediment. Geol. 183, 181–202.
Swart, P.K., 2015. The geochemistry of carbonate diagenesis: the past, present and future. Sedimentology 62, 1233–1304.
Swart, P.K., Melim, L.A., 2000. The origin of dolomites in tertiary sediments from the margin of Great Bahama Bank. J. Sediment. Res. 70, 738–748.
Tarutani, T., Clayton, R.N., Mayeda, T.K., 1969. The effect of polymorphism and magnesium substitution on oxygen isotope fractionation between calcium carbonate and water. Geochem. Cosmochim. Acta 33, 987–996.
Tribble, J.S., Arvidson, R.S., Lane, M., Mackenzie, F.T., 1995. Crystal chemistry, and thermodynamic and kinetic properties of calcite, dolomite, apatite, and biogenic silica: applications to petrologic problems. Sediment. Geol. 95, 11–37.
Tucker, M.E., Wright, V.P., 1990. Carbonate Sedimentology. Blackwell Scientific Publications, pp. 1–482.
Vahrenkamp, V.C., Swart, P.K., 1994. Late Cenozoic dolomites of the Bahamas: metastable analogues for the genesis of ancient platform dolomites. In: Purser, B.H., Tucker, M.E., Zenger, D.L. (Eds.), Dolomites: a Volume in Honour of Dolomieu, vol. 21. Int. Assoc. Sedimentol. Spec. Publ., pp. 133–153
Van Tuyl, F.M., 1916. New points on the origin of dolomite. Am. J. Sci. 42, 249–260.
Veizer, J., 1983. Chemical diagenesis of carbonates: theory and application of trace element technique. In: Arthur, M.A., Anderson, T.F., Kaplan, I.R., Veizer, J., Land, L. S. (Eds.), Stable Isotopes in Sedimentary Geology. Soc. Econ. Paleont. Mineral. Short Course, vol. 10, 3-1–3-100.
Vézina, J., Jones, B., Ford, D., 1999. sea-level highstands over the last 500,000 years: evidence from the Ironshore Formation on Grand cayman, British west indies. J. Sediment. Res. 69, 317–327.
Wang, R., Jones, B., Yu, K., 2019. Island dolostones: genesis by time-transgressive or event dolomitization. Sediment. Geol. 390, 15–30.
Wang, R., Yu, K., Jones, B., Wang, Y., Zhao, J., Feng, Y., Bian, L., Xu, S., Fan, T., Jiang, W., 2018a. Evolution and development of Miocene "island dolostones" on Xisha islands, south China sea. Mar. Geol. 406, 142–158.
Wang, Z., Huang, K., Zhang, D., You, L., Liu, X., Luo, W., 2018b. Maturation of neogene dolomite from xuande atoll of Xisha archipelago, the South China sea. Mar. Petrol. Geol. 92, 51–64.
Warren, J., 2000. Dolomite: occurrence, evolution and economically important associations. Earth Sci. Rev. 52, 1–81.
Wheeler, C.W., Aharon, P., Ferrell, R.E., 1999. Successions of late Cenozoic platform dolomites distinguished by texture, geochemistry, and crystal chemistry: Niue, South Pacific. J. Sediment. Res. 69, 239–255.
Woronick, R.E., Land, L.S., 1985. Late burial diagenesis, lower Cretaceous Pearsall and lower Glen Rose formations, south Texas. In: Schneidermann, N., Harris, P. (Eds.), Carbonate Cements, vol. 36. SEPM Spec. Publ, pp. 265–275.
Wu, S., Yang, Z., Wang, D., Lü, F., Lüdmann, T., Fulthorpe, C., Wang, B., 2014. Architecture, development and geological control of the Xisha carbonate platforms, northwestern South China Sea. Mar. Geol. 350, 71–83.
Xu, S., Yu, K., Fan, T., Jiang, W., Wang, R., Zhang, Y., Yue, Y., Wang, S., 2019. Coral reef carbonate $\delta^{13}C$ records from the northern South China Sea: a useful proxy for seawater $\delta^{13}C$ and the carbon cycle over the past 1.8 Ma. Global Planet. Change 182, 103003.
Yi, L., Jian, Z., Liu, X., Zhu, Y., Zhang, D., Wang, Z., Deng, C., 2018. Astronomical tuning and magnetostratigraphy of neogene biogenic reefs in Xisha islands, south China sea. Chin. Sci. Bull. 63, 564–573.
Zachos, J., Pagani, M., Sloan, L., Thomas, E., Billups, K., 2001. Trends, rhythms, and aberrations in global climate 65 Ma to present. Science 292, 686–693.
Zhai, S., Mi, L., Shen, X., Liu, X., Xiu, C., Sun, Z., Cao, J., 2015. Mineral compositions and their environmental implications in reef of Shidao Island, Xisha. Earth Sci. J. China Univ. Geosci. 40, 597–605 (in Chinese with English abstract).
Zhang, Y., Yu, K., Qian, H., 2018. LA-ICP-MS analysis of clinopyroxenes in basaltic pyroclastic rocks from the Xisha Islands, northwestern South China Sea. Minerals 8, 575.
Zhang, Y., Yu, K., Qian, H., Fan, T., Yue, Y., Wang, R., Jiang, W., Xu, S., Wang, Y., 2020. The basement and volcanic activities of the Xisha Islands: evidence from the kilometre-scale drilling in the northwestern South China Sea. Geol. J. 55, 571–583.
Zhao, H., Jones, B., 2012. Origin of "island dolostones": a case study from the Cayman Formation (Miocene), cayman brac, British west indies. Sediment. Geol. 243, 191–206.
Zhao, Q., 2010. The Sedimentary Research about Reef Carbonatite in Xisha Islands Waters. Ph.D. Thesis. Institute of Oceanology, Chinese Academy of Sciences, p. 158 pp (in Chinese with English Abstract).
Zhu, W., Xie, X., Wang, Z., Zhang, D., Zhang, C., Cao, L., Shao, L., 2017. New insights on the origin of the basement of the Xisha uplift, south China sea. Sci. China Earth Sci. 60, 2214–2222 (in Chinese with English Abstract).